JACS
JOURNAL OF THE AMERICAN CHEMICAL SOCIETY

ARTICLE

pubs.acs.org/JACS

Ultrahigh Mobility in Polymer Field-Effect Transistors by Design

Hoi Nok Tsao,[†] Don M. Cho,[†] Insun Park,[‡] Michael Ryan Hansen,[†] Alexey Mavrinskiy,[†] Do Y. Yoon,[‡] Robert Graf,[†] Wojciech Pisula,*[,†] Hans Wolfgang Spiess,[†] and Klaus Müllen*[,†]

[†]Max Planck Institute for Polymer Research, 55128 Mainz, Germany

[‡]Department of Chemistry, Seoul National University, Seoul 151-747, Korea

Supporting Information

ABSTRACT: In this article, the design paradigm involving molecular weight, alkyl substituents, and donor−acceptor interaction for the poly[2,6-(4,4-bis-alkyl-4*H*-cyclopenta-[2,1-b;3,4-b′]-dithiophene)-*alt*-4,7-(2,1,3-benzothiadiazole)] (cyclopentadithiophene−benzothiadiazole) donor−acceptor copolymer (CDT−BTZ) toward field-effect transistors (FETs) with ultrahigh mobilities is presented and discussed. It is shown that the molecular weight plays a key role in improving hole mobilities, reaching an exceptionally high value of up to 3.3 $cm^2 V^{-1} s^{-1}$. Possible explanations for this observation is highlighted in conjunction with thin film morphology and crystallinity. Hereby, it is found that the former does not change, whereas, at the same time, crystallinity improved with ever growing molecular weight. Furthermore, other important structural design factors such as alkyl chain substituents and donor−acceptor interaction between the polymer backbones potentially govern intermolecular stacking distances crucial for charge transport and hence for device performance. In this aspect, for the first time we attempt to shed light onto donor−acceptor interactions between neighboring polymer chains with the help of solid state nuclear magnetic resonance (NMR). On the basis of our results, polymer design principles are inferred that might be of relevance for prospective semiconductors exhibiting hole mobilities even exceeding 3 $cm^2 V^{-1} s^{-1}$.

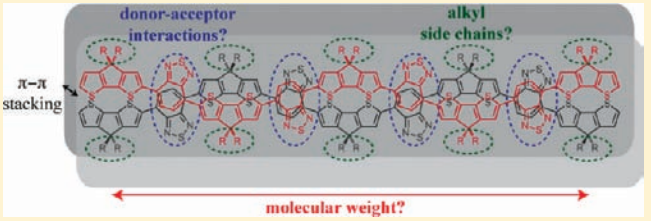

1. INTRODUCTION

The realization and commercialization of plastic electronics like flexible displays or smart tags call for organic semiconductors that can be easily processed into thin films and show field-effect transistor (FET) charge carrier mobilities exceeding 0.1 $cm^2 V^{-1} s^{-1}$.[1,2] Owing to their facile film formation, soluble polymer semiconductors provide the desired ready processability needed for fast printing processes required for cheap organic devices.[3] Their mechanical flexibility provides an additional advantage for bendable electronics compared to fragile small-molecule single-crystal FETs.[4] However, charge carrier mobilities in polymer devices are generally low as a result of the poor packing and lack of macroscopic order of those materials. There have been several approaches toward enforcing thin film crystallinity in order to solve this problem.[5,6] One major strategy was, for instance, to impart molecular arrangement by the regioregular placement of alkyl chains in polythiophenes.[7−9] Other possibilities are insulator surface treatments[10,11] or proper processing techniques such as dip-coating[12−14] or zone-casting[15−18] that can be utilized to achieve enhanced long-range molecular order. In this article, focus is turned to three major polymer design principles whose contributions to enhancing **P1** (Figure 1)-based FET performance are illustrated, namely the influence of (i) intermolecular donor−acceptor interactions, (ii) the molecular weight, and (iii) alkyl substituents.

(1) In contrast to homopolymers such as P3HT, **P1** is a copolymer consisting of an alternating arrangement of cyclopentadithiophene (CDT) as a donor and benzothiadiazole (BTZ) as an acceptor unit. The low band gap of **P1** makes it attractive for applications in organic photovoltaic cells.[19,20] Moreover, the planar arrangement of the conjugated backbone ensures a close π-stacking distance, which is relavant for efficient intermolecular charge carrier transport. It was assumed that the close packing of the polymer chains might originate from assisting donor−acceptor interactions. In this work, for the first time for such macromolecular systems, solid-state nuclear magnetic resonance (NMR) provides a picture of the packing mode and indicates that additional forces besides π-stacking do not seem to contribute to the noncovalent interactions and polymer organization.

(2) Another potential factor influencing polymer FET behavior is the molecular weight as has been particularly well demonstrated for regioregular poly(3-hexylthiophene) (P3HT).[21−24] We have previously shown for **P1** that higher molecular weights, expressed in number average molecular weight M_n, led to increased macroscopic order and therefore elevated hole mobilities as compared to the lower M_n case, where inferior FET performance was observed with pronounced macroscopic disorder. Further enforcement of the long-range order by directional alignment

Received: October 1, 2010
Published: February 3, 2011

dx.doi.org/10.1021/ja108861q | *J. Am. Chem. Soc.* 2011, 133, 2605–2612

of the **P1** polymer chains reached a hole mobility of up to 1.4 $cm^2 V^{-1} s^{-1}$, one of the highest values reported so far for polymeric systems.[25] Just recently, new conjugated polymers have been reported with mobilities around 1 $cm^2 V^{-1} s^{-1}$.[26,27] The question remains to what extent the morphology of **P1**, which is a more planar and rigid macromolecule than, for instance, P3HT, is influenced by the molecular weight and how the charge carrier transport in FETs is affected by these two aspects. Particularly, it is scrutinized how a further increase in M_n leads to an additional boost in hole mobility of up to 3.3 $cm^2 V^{-1} s^{-1}$.

(3) As a further design aspect, alkyl substituents of this CDT−BTZ copolymer are taken into consideration, which can dramatically alter transistor performances.[28] Building up on our previous findings of **P1** in which both polymer chain length expressed in a high M_n and close π-stacking distance are crucial for efficient charge transport,[25] the hexadecyl (C_{16}) substituent of **P1** was replaced by a more abridged 3,7-dimethyloctyl ($C_{8,2}$) intending to achieve a shorter intermolecular $\pi-\pi$ separation. The M_n effects on crystallinity, morphology and transistor behavior of this CDT−BTZ−$C_{8,2}$ polymer (**P2** in Figure 1) are illustrated as well.

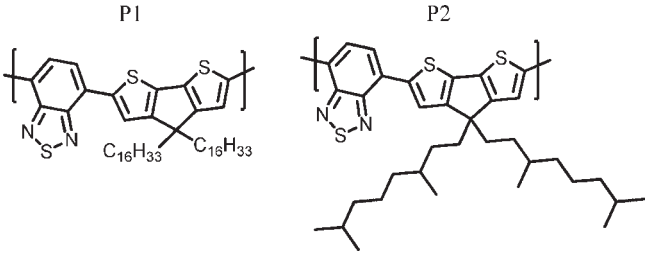

Figure 1. Chemical structures of CDT−BTZ−C_{16} (**P1**) and CDT−BTZ−$C_{8,2}$ (**P2**).

Table 1. M_n-Dependent FET Performance of Both P1 and P2

Polymer	M_n [g/mol][a]	μ_{sat} [$cm^2/(V\,s)$][b]	I(on)/I(off)
P1	13K (11 K)	0.28 (0.26)	10^3-10^4
P1	30K (16K)	0.59 (0.50)	10^3-10^4
P1	51K (25 K)	1.2 (0.94)	10^2-10^4
P1	(35 K)	3.3 (2.62)	10^5-10^6
P2	1.8 K	0.016 (0.014)	10^4
P2	6.5 K	0.20 (0.19)	10^3-10^5
P2	16 K	0.40 (0.34)	10^2-10^3

[a] M_n values were obtained using PS/THF standards. M_n values in parentheses were obtained from PS/TCB GPC standard. [b] Numbers listed for μ_{sat} represent maximum hole mobilities measured, whereas the values in parentheses reveal averaged hole mobilities from 10 devices.

2. RESULTS AND DISCUSSION

Molecular Weight-Dependent FET Performance. All FETs were fabricated employing the bottom-gate, bottom-contact architecture. The 200 nm thick SiO_2 dielectric covering the highly doped Si acting as the gate electrode was functionalized with hexamethyldisilazane (HMDS) to minimize interfacial trapping sites. Polymer thin films were deposited by drop-casting 2 mg mL^{-1} o-dichlorobenzene solution on FET substrates heated at 100 °C in nitrogen atmosphere, followed by annealing at 200 °C for 1 h. The channel lengths and widths are 20 and 1400 μm, respectively. For the average mobilities, 10 transistors were measured in nitrogen atmosphere. Table 1 depicts the transistor performances in dependence of M_n for both **P1** and **P2**. Clearly, the hole mobilites scale with elevated M_n for both alkyl chain versions, with an unprecedented high hole mobility of up to μ = 3.3 $cm^2 V^{-1} s^{-1}$ for the highest M_n of **P1** as derived from the transistor characteristics exhibited in Figure 2a,b. Note that this polymer bearing the best FET performance was too poorly soluble to dissolve in tetrahydrofuran (THF) for the standard polystyrene (PS)/THF gel permeation chromatography (GPC) molecular weight measurements conducted for the other polymer systems shown. To circumvent this hurdle, 1,2,4-trichlorobenzene (TCB) instead of THF had to be employed for the GPC. For reasons of comparability, GPC was also measured in PS/TCB standard for the other more soluble **P1** batches, with the resulting M_n values illustrated in parentheses in Table 1. In the remainder of this article, all M_n of **P1** mentioned in the text refer to this PS/TCB standard. Figure 3a is a graphical illustration of the average hole mobility dependence on M_n. To gain

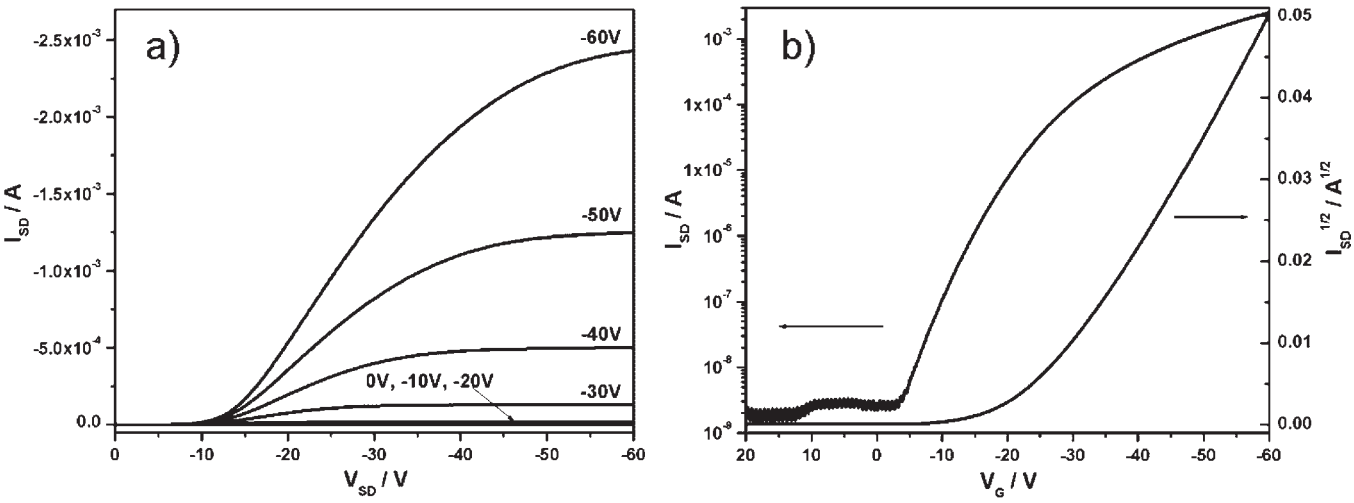

Figure 2. (a) Output characteristics at various gate biases V_G and (b) transfer curve at a source drain bias of V_{SD} = −60 V for **P1** FET with the highest M_n = 35 kg mol^{-1} (PS/TCB standard).

dx.doi.org/10.1021/ja108861q | J. Am. Chem. Soc. 2011, 133, 2605–2612

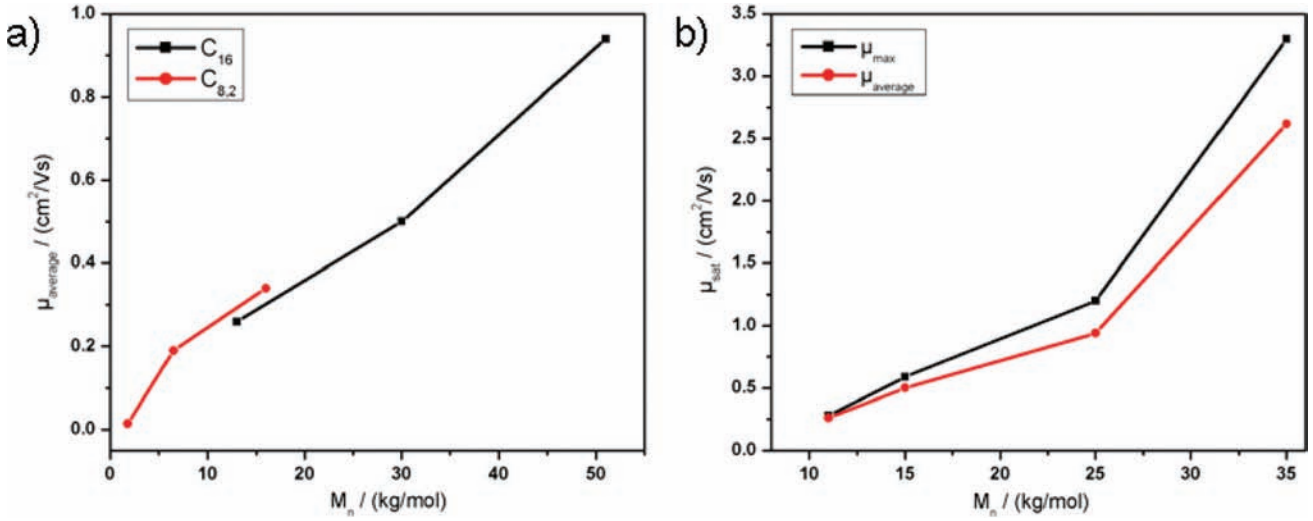

Figure 3. (a) Graphical illustration of M_n (PS/THF standard)-dependent average saturated hole mobilites $\mu_{average}$ for both **P1** and **P2**. (b) Graphical illustration of M_n (PS/TCB standard)-dependent average $\mu_{average}$ and maximum μ_{max} saturated hole mobilities for **P1**.

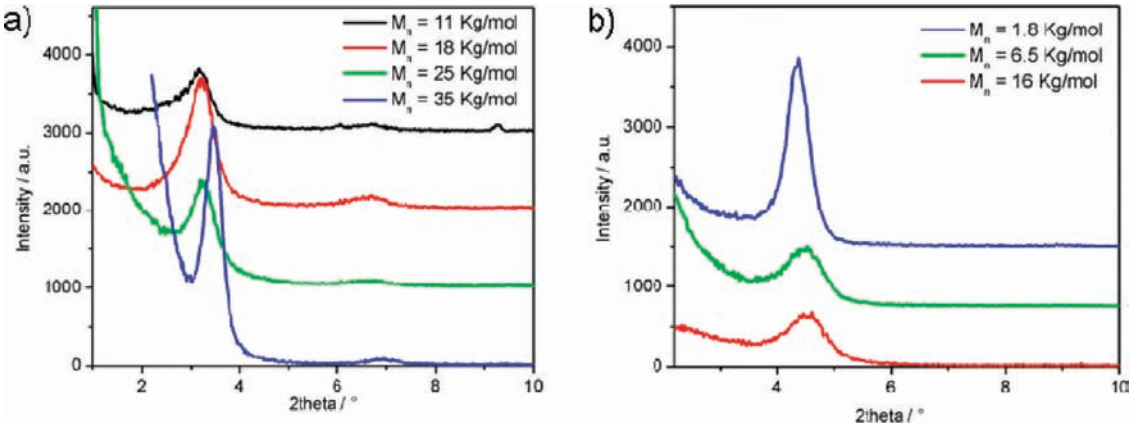

Figure 4. XRD of (a) **P1** and (b) **P2** thin films of various M_n.

information about the change in hole mobility of both **P1**- and **P2**-based FETs at comparable M_n values, data from the PS/THF standard were plotted, leaving out the highest M_n of **P1** for which the PS/THF standard could not be applied. Unfortunately, much inferior molecular weights of **P2** were attained compared to **P1** (Table 1) due to solubility problems of the former. In fact, the maximum M_n achievable for **P2** is just slightly above the lowest M_n of **P1** (Figure 3a, Table 1), rendering direct comparison of the alteration of μ with M_n of both polymers ambiguous. Nevertheless, hole mobilities also scale up with growing M_n for the **P2** devices. More precisely, at comparable M_n for both **P1** and **P2**, the hole mobilities are similar as well (Figure 3a). It seems that these two different alkyl chains do not alter charge carrier mobility, at least for the specific M_n region we are able to look at.

At this point it is interesting to deduce a more profound relationship between molecular weight and hole mobility of the **P1** film. The M_n-dependent rise of μ is plotted in Figure 3b for both the maximum and average mobilities. The increase of μ follows linearly with elevated M_n for the first three low M_n values, whereas a more sudden jump in μ occurs for the highest M_n values, suggesting a more dramatic rise in hole mobility for ever growing molecular weights. On the basis of these data, it is anticipated that the hole mobility of μ = 3.3 $cm^2\ V^{-1}\ s^{-1}$ obtained in our highest M_n system can even be further surpassed for additional M_n growth, keeping in mind that this extraordinary FET performance is not optimized yet. This is evident when considering Figure 2a,b illustrating the output and transfer characteristics of this **P1** device, respectively. As can be seen from the nonlinear rise of the current at low V_{SD} from the output curves (Figure 2a), a huge contact resistance is present.[29] The origin of this contact resistance can be high disorder at or poor contacts of the copolymer film with the source and drain electrodes. The latter hypothesis is supported by the fact that the polymer film can be completely stripped of the bottom contact transistor substrate, highlighting the lack of strong layer adhesion on both the dielectric surface and the source and drain electrodes. Elimination of the contact resistance is expected to provide hole mobilities even beyond 3.3 $cm^2\ V^{-1}\ s^{-1}$.

Molecular Weight Dependent Thin Film Crystallinity and Intermolecular π-Stacking. The most obvious explanation for the observed gain in hole mobility with growing molecular weights is a possible improvement in thin film crystallinity since more pronounced long-range order facilitates charge carrier

dx.doi.org/10.1021/ja108861q | J. Am. Chem. Soc. 2011, 133, 2605–2612

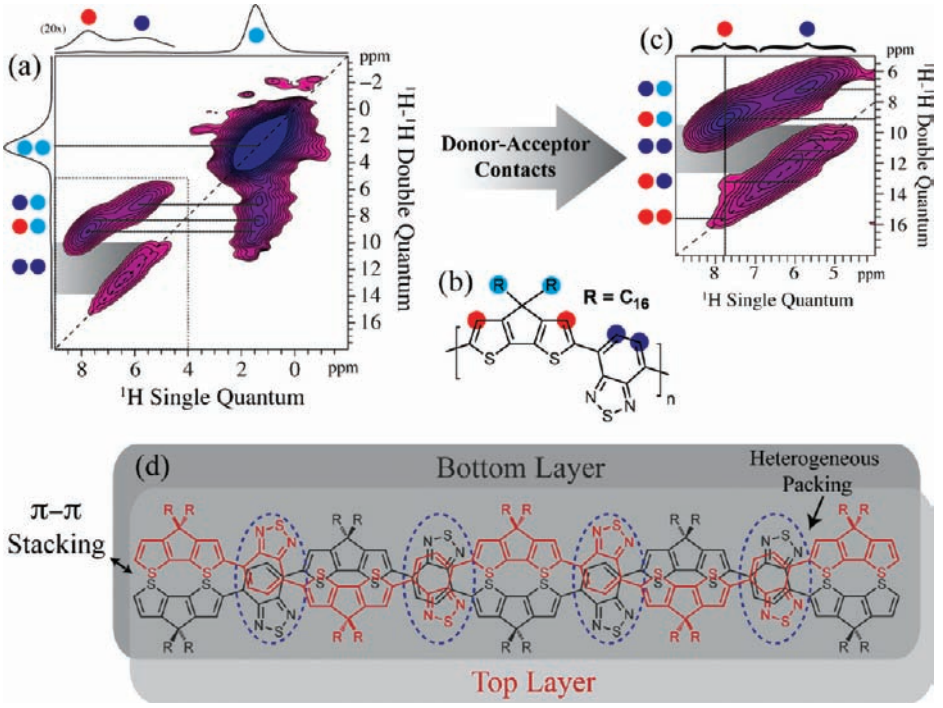

Figure 5. Local packing and organization of donor−acceptor groups in **P1** with M_n = 35 kg mol^{-1}. (a) 2D contour plot of the ^{1}H−^{1}H DQ-SQ correlation spectrum recorded at 20.0 T using a back-to-back recoupling/reconversion time of 2 rotor periods and a spinning frequency of 30.0 kHz. (b) Color scheme used for assignments. (c) Expansion of the backbone region (dashed box in panel a) showing the contacts between donor and acceptor groups. (d) Schematic drawing illustrating the local packing of donor−acceptor groups in two neighboring BTZ−CDT copolymer chains (here denoted as "layers"). The dashed circles (blue) mark the regions where the acceptors groups are heterogeneously packed on top of one another.

transport.[30,31] Hence, to investigate the molecular weight-dependent macroscopic order of the CDT−BTZ copolymers **P1** and **P2** in thin film, X-ray diffraction (XRD) was conducted on drop-cast layers on HMDS-treated SiO_2 prepared in the same way as the device fabrication. For all compounds studied, one diffraction peak was present, suggesting a tendency for macroscopic order (Figure 4). In the case of **P1**, a small and broad second-order peak for the various M_n was observed, indicating a higher order in the bulk films as compared to **P2** layers for which these second-order peaks were missing. On the basis of these XRD results, lamella packing of the polymer chains can be deduced for all copolymers.[32−34] Differences in the degree of macroscopic order among the two copolymers themselves in terms of varying M_n values were also revealed. For instance, considering the **P1** films, the XRD diffraction peak for the highest M_n (35 kg mol^{-1}, blue curve in Figure 4a) is narrower than the other three lower M_n values, alluding to a more pronounced long-range order for the former case. This observation is a plausible explanation for the sudden rise in hole mobility of **P1** at this highest M_n (Figure 3b). Moreover, due to higher crystallinity, especially of the alkyl substituents, the chain-to-chain distance between backbones decreases from 2.78 to 2.70 nm for M_n = 11−25 kg mol^{-1} to 2.56 nm for M_n = 35 kg mol^{-1}. This fact possibly opens up additional charge transport pathways via the alkyl chain other than along the π-stacking direction in a lamella packing, potentially improving carrier mobility.[7,35]

For **P2** on the other hand, thin film macroscopic order of the three molecular weights showed the reverse behavior. Here, the diffraction peak is not as broadened for the lowest M_n as for the other two higher molecular weights (Figure 4b), indicating increased thin film crystallinity for the lowest M_n. This trend makes sense when utilizing the same reasoning proposed for P3HT whose thin film crystallinity exhibits similar M_n dependence. For P3HT, the kinetics of shorter and thus more agile molecules is held responsible for the ability to self-assemble in more crystalline superstructures.[21,36,37] This explanation fits as well to the M_n behavior of **P2**. However, care has to be taken here when comparing **P2** with **P1**. Note that this higher crystallinity was observed for the lowest M_n of **P2**, about 1 order of magnitude lower than the shortest polymer chains synthesized for **P1**. Therefore, it cannot be excluded that a more crystalline packing in bulk thin film of **P1** with comparably low M_n as for **P2** will be present as well. Similarly, there is no reason for ruling out that a comparably high M_n of 35 kg mol^{-1}as achieved for **P1** will not lead to enhanced crystallinity for **P2** as well. Nevertheless, what is most striking about the CDT−BTZ copolymers is that macroscopic order does not seem to diminish with increasing M_n, a feature that only few other polymers share as well.[38] P3HT for instance shows the opposite trend, with thin film crystallinity decreasing with growing molecular weights. This behavior was explained by the sluggishness of the longer polymer chains, being unable to self-assemble effectively anymore. Apparently, this reasoning does not seem to apply for the CDT−BTZ copolymers. The mechanisms behind the maintenance and even improved crystallinity with higher M_n of **P1** and **P2** are still not understood. One possible explanation might be improved donor−acceptor interaction between the more extended backbones containing a higher number of donor and acceptor units at elevated M_n and hence possibly forcing the more inert longer chains into higher long-range arrangement. To verify this hypothesis, molecular scale information about the local packing and organization of donor−acceptor groups in the condensed state

of **P1** with the highest M_n showing the most distinct thin film crystallinity is obtained from solid-state NMR. This method probes the local environments of the individual nuclei selectively through short-ranged nuclear spin interactions, e.g., dipole−dipole and chemical shift interactions, which are sensitive to the specific local packing arrangements.[39−41] The results from applying this approach to the condensed state of **P1** with the highest M_n, which exhibits the most distinct thin film crystallinity, are shown in Figure 5. The site-specific local packing information is obtained via two-dimensional (2D) $^1H-^1H$ double-quantum single-quantum (DQ-SQ) correlation spectroscopy.[42,43] The structural information is encoded in the appearance and location of the NMR correlation peaks in the 2D spectrum in Figure 5. First, the presence of $\pi-\pi$ stacking for the BTZ−CDT copolymer backbone can clearly be observed via the autocorrelation peak at SQ_{iso} = 5−7.5 ppm and DQ_{iso} = 10−15 ppm for the BTZ protons (see assignment in Figure 5b), displaying an elongation toward lower frequency that is characteristic of $\pi-\pi$ stacking in aromatic-based systems.[44] Second, this line shape appears to be split, which illustrates that the packing of the BTZ groups is heterogeneous throughout the sample. The protons of the CDT groups on the other hand do not show this kind of elongation or splitting, indicating that $\pi-\pi$ stacking effects do not affect these groups to the same extent as compared to the BTZ acceptor groups. However, they do show a strong correlation with the directly attached side chains and also a direct correlation with the protons of the acceptor group within the copolymer chain (see Figure 5c). Combining these structural features gives the local packing arrangement of donor−acceptor groups as illustrated in Figure 5d that is consistent with the XRD measurements in Figure 4a. In this model, donor−acceptor groups are $\pi-\pi$ stacked in a lamellar kind of fashion, and these groups are ordered in an alternating way as shown in Figure 5d. Thereby, the acceptor groups in one layer are located on top of the acceptor groups in adjacent layers, however, not always in the exact same position, leading to a heterogeneous packing. This model also allows for optimal packing of the side chains that, in the case of long and bulky alkyl chains (C_{16}) as used here, should be beneficial in order to avoid steric clash. Conclusively, solid-state NMR does not reveal a donor−acceptor overlap within 0.4 nm.[45,46] Thus, donor−acceptor interaction between the neighboring interchain CDT and BTZ moieties does not seem to occur as assisting noncovalent driving forces for the observed improvement in thin film crystallinity with increasing M_n of **P1**, alluding to the complexity of this CDT−BTZ copolymer system. This implies that the enhanced packing order resulting in improved thin film crystallinity with increasing M_n of **P1** results from π-stacking interactions of the planar extended conjugated backbones only.

Elevated long-range order with growing M_n, as discussed so far, might not be the only cause for the ever rising hole mobility. Another important factor that affects charge transport is the intermolecular π-stacking distance.[47−49] To gain a deeper insight into M_n and alkyl chain (C_{16} and $C_{8,2}$) dependent intermolecular π-stacking distances, which provide a hint to intermolecular charge carrier hopping important for charge carrier mobility, 2D wide-angle X-ray scattering (2D-WAXS) of extruded fibers of **P1** with various M_n was conducted (Figure 6a,b,c). For the three molecular weights studied, no significant change in π-stacking distances (0.37−0.38 nm) was measured, suggesting that this parameter is not dependent on M_n. Since the alkyl chains attached to the CDT unit extend out of plane of the polymer backbone, π-stacking is expected to be influenced by the alkyl substituents. Conclusively, the shorter $C_{8,2}$ chains should lower steric hindrance and thus enable closer intermolecular π-stacking for higher charge carrier mobilities since in our previous study we have shown that close intermolecular π-stacking yields hole mobilities larger than 0.1 $cm^2/(V\ s)$ despite the lack of macroscopic order.[50] In this aspect, 2D-WAXS of the highest M_n **P2** extruded fiber was measured (Figure 6d), revealing the same $\pi-\pi$ distance of 0.37 nm as for **P1**. Apparently, shortening the alkyl chain length by a factor of 2 does not trigger any change in intermolecular packing, prompting us to believe that either the minimal π-stacking distance has already been achieved, or even further abridged aliphatic chains have to be introduced to depress steric hindrance. However, the alkyl chains were not shortened once again since this will dramatically lower solubility and hence processability as well as prevent the synthesis of higher molecular weights. Therefore, possible alteration of intermolecular face-to-face separation is not the cause for the constant rise of hole mobility with growing molecular weight.

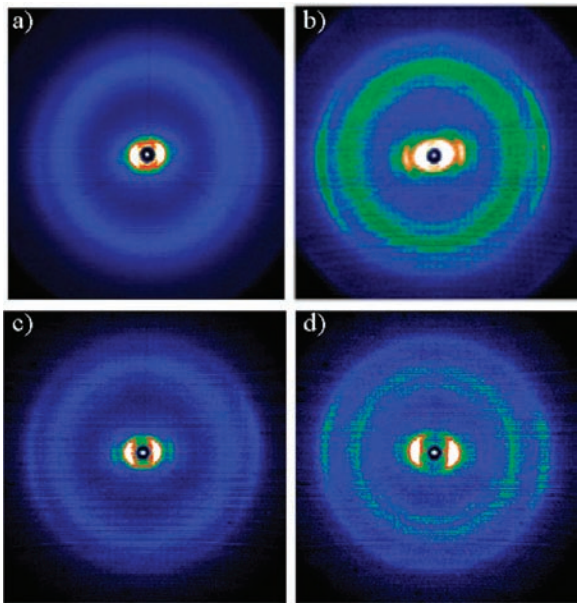

Figure 6. 2D-WAXS of extruded fibers of (a) **P1** with M_n = 11 kg mol^{-1}, (b) **P1** with M_n = 25 kg mol^{-1}, (c) **P1** with M_n = 35 kg mol^{-1}, and (d) **P2** with M_n = 16 kg mol^{-1}.

Molecular Weight-Dependent Polymer Thin Film Morphology. Besides the previously presented structural analysis of thin film crystallinity (XRD) and of bulk (2D-WAXS), film morphologies are essential as well for understanding transistor behavior.[51−54] In order to highlight the M_n dependent thin film morphologies of both **P1** and **P2**, we start with the lowest molecular weights, which were obtained from **P2**. As the atomic force microscope (AFM) image on the lowest **P2** FET sample (same as that used for transistor measurements) reveals (Figure 7a), randomly oriented fibers are present. Taking a closer look at this layer by scanning a smaller area, a distribution of elongated and curled nanofibers can be found (Figure 7b) where the degree of curling varies. With further increase of molecular weights, the morphology changes, with the transition from randomly distributed curled fibers into elongated ones being densely packed parallel next to each other, in this way forming fibrous crystallites that span over the whole film.

This film topography prevails with continuously growing molecular weights as was achieved for **P1**. Independent of M_n, **P1** thin films contain fibrous crystallites and therefore no change in morphology can be observed (Figure 8). However, with increasing M_n, those crystallites seem to become slightly more extended on average as can be deduced when comparing panels a−d of Figure 8 where the fibrous crystallite texture evolves more distinctly. Figure 8e provides a more detailed image of the typical crystallites that take the shape of fibers densely packed next to each other. In fact, for comparable M_n, the morphology of both **P2** (Figure 7c) and **P1** (Figure 8a) are similar, marked by the predominant existence of fibers, prompting us to believe that the type of alkyl chains introduced in our systems does not influence morphology.

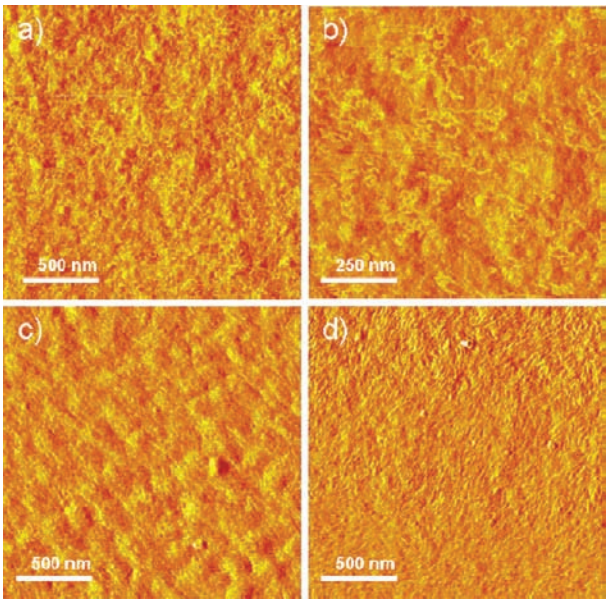

Figure 7. AFM images of **P2** FET thin films drop-cast from M_n of (a,b) 1.8 kg mol^{-1}, (c) 6.5 kg mol^{-1}, and (d) 16 kg mol^{-1}. Image b is a more detailed AFM scan of image a, revealing curled polymer fibers.

The best hole mobility measured for the FETs fabricated with the maximum M_n **P1** rather suggests that the increase in μ is originated from the highest crystallinity of this film compared to all other molecular weight layers as revealed by XRD studies (Figure 4a). While pronounced crystallinity is a reasonable explanation for the rise of hole mobility with growing M_n for **P1**, the same reasoning does not hold true for **P2**. This aspect is underlined by the transistor behaviors of the **P2** copolymers for which the smallest M_n device showed more enhanced crystallinity as indicated by a narrower XRD diffraction peak (Figure 4b) but lower hole mobilities as compared to the other two higher M_n FETs, opposite to what has been observed for **P1**. This effect possibly originates from the different thin film morphologies of **P2.** Despite its high crystallinity, the lowest M_n layer of **P2** consists of curled and randomly distributed fibers (Figure 7a,b), resulting in lower long-range order, in this way reducing charge transport as compared to the higher M_n films which more resemble the densely packed fribrous crystalline domains characteristic for **P1** (Figure 7c,d, 8), highlighting the importance of thin film morphology. In fact, when taking a closer look at M_n-dependent evolution of **P1** film morphology, no dramatic change takes place (Figure 8). Obviously, the enhancement of charge carrier mobility is not triggered by a significant extension of crystalline domains coming along with morphology transformation as has been reported for other polymer systems.[55] This remarkable feature leads to the assumption that two additional phenomena having no influence on morphology and crystallinity might play a key role as well for the increase of mobility with growing molecular weights. Generally, higher molecular weight means, on average, the presence of longer polymer chains with two implications. First, extended polymer chains can promote interconnectivity between neighboring crystalline fiber domains, reducing grain boundaries and thus facilitating charge carrier transport as has been for instance proposed for P3HT.[56,57] Polymer films with higher macroscopic

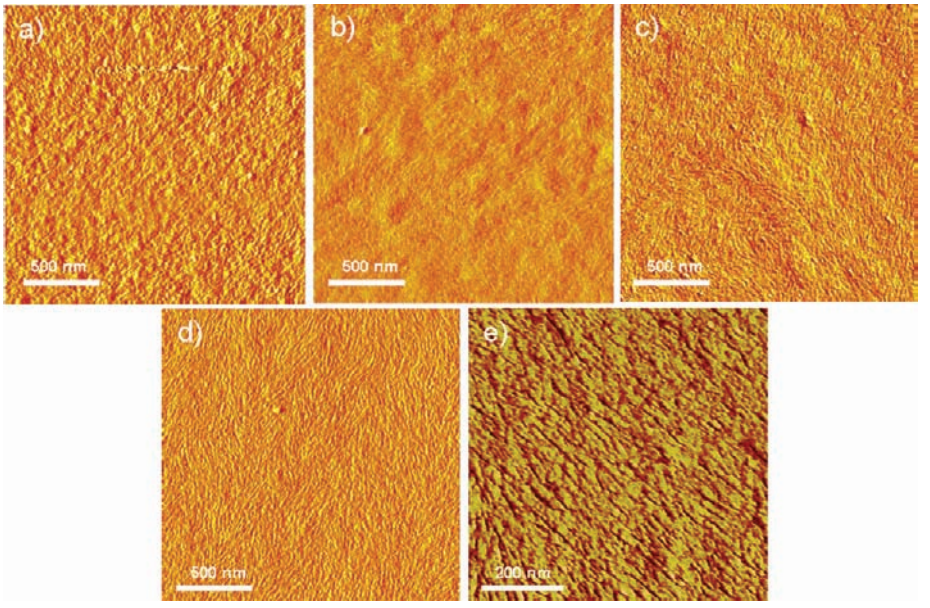

Figure 8. AFM images of **P1** FET thin films drop-cast from M_n (PS/TCB standard) of (a) 11 kg mol^{-1}, (b) 18 kg mol^{-1}, (c) 25 kg mol^{-1}, and (d) 35 kg mol^{-1}. (e) Zoomed in image of d detailing the fibrous crystalline domains.

order marked by an invariant morphology containing small crystal domain sizes have been shown to trigger grain boundary smoothing as well, leading to improved charge carrier mobilities.[58,59] This aspect serves as a further alternative explanation for the outstanding mobility observed for **P1** with the highest M_n for which the highest thin film crystallinity and hence macroscopic order was found without a change in morphology. Contrarily, this degree of grain boundary reduction is not anticipated for the lowest M_n case, namely, the **P2** film where randomly oriented curled fibers were present (Figure 7a,b). Even though better crystallinity in this thin film exists as compared to the higher M_n layers, the lack of domain connectivity in combination with low macroscopic order might explain the measured inferior hole mobility. Second, in our previous work on anisotropic carrier transport in directionally aligned **P1** films, there is strong indication that charge carrier transport along the **P1** backbone is fastest as compared to $\pi-\pi$ charge transfer.[25,60] Therefore, the longer high M_n polymer chains do not only reduce grain boundaries but also potentially promote fast carrier transport between neighboring fibers and hence support high transistor performance. Given the observation that the fiber-like morphology remains for all studied M_n films and that those fibers consist of lamella packed polymer chains with their backbones aligned along the fiber long axis, it is reasonable to expect that the longer the polymer chains at higher M_n, the more the chain-to-chain trapping sites along the fiber axis are reduced within a fibrous crystallite. That is, for comparable fibers (in length), the ones that are made of shorter polymer chains will most probably contain more trapping sites than the ones consisting of longer molecules. In this sense, the longer polymer chains trigger the formation of fibers that themselves contain less trapping sites along the fiber axis and hence prospectively lead to better charge transport. Surely, charge transport in these nondirectionally oriented films is not only taking place along the polymer backbones but is rather a superposition of carrier movement along the π-stacking and the polymer backbone directions. Nevertheless, reduction of trapping sites within the individually ordered fibers can still significantly contribute to higher charge carrier mobilities in this CDT−BTZ system.

3. CONCLUSION

In this work design principles toward ultrahigh mobility FETs based on the CDT−BTZ donor−acceptor copolymer have been evaluated and discussed. Even though solid-state NMR could not unambiguously prove the existence of donor−acceptor interactions expected to be beneficial for improved crystallinity, it has been, on the other hand, more vividly demonstrated that a powerful tool for achieving extraordinary charge carrier mobilities in polymer FETs is the molecular weight. Thin films of both compounds **P1** and **P2** exhibit a steady rise in hole mobility in FETs with an increasing number average molecular weight M_n. Except for the low M_n case of **P2**, film morphologies do not change with growing M_n as well, avoiding the necessity of controlling morphology in order to optimize charge transport. Furthermore, this invariance of film morphology can be interpreted as an indirect evidence for pronounced crystallite connectivity and promoted fast charge transport along polymer backbones, both factors that additionally support the measured state-of-the-art transistor performance. More strikingly, enhanced crystallinity was observed for the highest M_n CDT−BTZ−C_{16} (**P1**) copolymer layer, contradicting the common belief that with rising M_n and polymer chain inertness, thin film order is inhibited. On the basis of our results, it is predicted that further elevation of the molecular weight might potentially improve thin film crystallinity without deterioration of film morphology, ultimately leading to unprecedented hole mobilities for polymer FETs.

■ ASSOCIATED CONTENT

Supporting Information. Complete ref 38 and experimental details. This material is available free of charge via the Internet at http://pubs.acs.org.

■ AUTHOR INFORMATION

Corresponding Author

*E-mail: pisula@mpip-mainz.mpg.de (W.P.); muellen@mpip-mainz.mpg.de (K.M.).

■ ACKNOWLEDGMENT

The authors thank Michael Steiert for XRD measurements and Marcel Kastler, Xinliang Feng, Martin Baumgarten, and Jens Wenzel Andreasen for very helpful discussions. We also acknowledge the support of the International Research Training Group (IRTG), jointly funded by the German Research Foundation (DFG) and the National Research Foundation of Korea (NRF).

■ REFERENCES

(1) Arias, A. C.; MacKenzie, J. D.; McCulloch, I.; Rivnay, J.; Salleo, A. *Chem. Rev.* **2010**, *110*, 3–24.
(2) Leenen, M. A. M.; Arning, V.; Thiem, H.; Steiger, J.; Anselmann, R. *Phys. Status Solidi A* **2009**, *206*, 588–597.
(3) Yan, H.; Chen, Z. H.; Zheng, Y.; Newman, C.; Quinn, J. R.; Dötz, F.; Kastler, M.; Facchetti, A. *Nature* **2009**, *457*, 679–686.
(4) Forrest, S. R. *Nature* **2004**, *428*, 911–918.
(5) Tsao, H. N.; Müllen, K. *Chem. Soc. Rev.* **2010**, *39*, 2372–2386.
(6) Liu, S.; Wang, W. M.; Briseno, A. L.; Mannsfeld, S. C. B.; Bao, Z. *Adv. Mater.* **2009**, *21*, 1–16.
(7) Sirringhaus, H.; Brown, P. J.; Friend, R. H.; Nielsen, M. M.; Bechgaard, K.; Langeveld-Voss, B. M. W.; Spiering, A. J. H.; Janssen, R. A. J.; Meijer, E. W.; Herwig, P.; de Leeuw, D. M. *Nature* **1999**, *401*, 685–688.
(8) McCullough, R. D.; Lowe, R. D. *J. Chem. Soc., Chem. Commun.* **1992**, *1*, 70–72.
(9) Katz, H. E.; Bao, Z.; Gilat, S. L. *Acc. Chem. Res.* **2001**, *34*, 359–369.
(10) Meredig, B.; Salleo, A.; Gee, R. *ACS Nano* **2009**, *3*, 2881–2886.
(11) Kim, D. H.; Jang, Y.; Park, Y. D.; Cho, K. *Langmuir* **2005**, *21*, 3203–3206.
(12) Wang, G.; Swensen, J.; Moses, D.; Heeger, A. J. *J. Appl. Phys.* **2003**, *93*, 6137–6141.
(13) Liu, N.; Zhou, Y.; Wang, L.; Peng, J.; Wang, J.; Pei, J.; Cao, Y. *Langmuir* **2009**, *25*, 665–671.
(14) Li, L.; Gao, P.; Schuermann, K. C.; Ostendorp, S.; Wang, W.; Du, C.; Lei, Y.; Fuchs, H.; De Cola, L.; Müllen, K.; Chi, L. *J. Am. Chem. Soc.* **2010**, *132*, 8807–8809.
(15) Pisula, W.; Menon, A.; Stepputat, M.; Lieberwirth, I.; Kolb, U.; Tracz, A.; Sirringhaus, H.; Pakula, T.; Müllen, K. *Adv. Mater.* **2005**, *17*, 684–688.
(16) Miskiewicz, P.; Mas-Torrent, M.; Jung, J.; Kotarba, S.; Glowacki, I.; Gomar-Nadal, E.; Amabilino, D. B.; Veciana, J.; Krause, B.; Carbone, D.; Rovira, C.; Ulanski, J. *Chem. Mater.* **2006**, *18*, 4724–4729.

(17) Duffy, C. M.; Andreasen, J. W.; Breiby, D. W.; Nielsen, M. M.; Ando, M.; Minakata, T.; Sirringhaus, H. *Chem. Mater.* **2008**, *20*, 7252–7259.
(18) Tracz, A.; Makowski, T.; Masirek, S.; Pisula, W.; Geerts, Y. H. *Nanotechnology* **2007**, *18*, 485303.
(19) Peet, J.; Kim, J. Y.; Coates, N. E.; Ma, W. L.; Moses, D.; Heeger, A. J.; Bazan, G. C. *Nat. Mater.* **2007**, *6*, 497–500.
(20) Kim, J. Y.; Lee, K.; Coates, N. E.; Moses, D.; Nguyen, T.-Q.; Dante, M.; Heeger, A. J. *Science* **2007**, *317*, 222–225.
(21) Kline, R. J.; McGehee, M. D.; Kadnikova, E. N.; Liu, J.; Fréchet, M. J. *Adv. Mater.* **2003**, *15*, 1519–1522.
(22) Zen, A.; Pflaum, J.; Hirschmann, S.; Zhuang, W.; Jaiser, F.; Asawapirom, U.; Rabe, J. P.; Scherf, U.; Neher, D. *Adv. Funct. Mater.* **2004**, *14*, 757–764.
(23) Verilhac, J.-M.; LeBlevennec, G.; Djurado, D.; Rieutord, F.; Chouiki, M.; Travers, J. P.; Pron, A. *Synth. Met.* **2006**, *156*, 815–823.
(24) Zhang, R.; Li, B.; Iovu, M. C.; Jeffries-El, M.; Sauvé, G.; Cooper, J.; Jia, S.; Tristram-Nagle, S.; Smilgies, D. M.; Lambeth, D. N.; McCulloch, R. D.; Kowalewski, T. *J. Am. Chem. Soc.* **2006**, *128*, 3480–3481.
(25) Tsao, H. N.; Cho, D.; Andreasen, J. W.; Rouhanipour, A.; Breiby, D. W.; Pisula, W.; Müllen, K. *Adv. Mater.* **2009**, *21*, 209–212.
(26) Li, Y.; Singh, S. P.; Sonar, P. *Adv. Mater.* **2010**, *22*, 4862–4866.
(27) Zhang, W.; Smith, J.; Watkins, S. E.; Gysel, R.; McGehee, M.; Salleo, A.; Kirkpatrick, J.; Ashraf, S.; Anthopoulos, T.; Heeney, M.; McCulloch, I. *J. Am. Chem. Soc.* **2010**, *132*, 11437–11439.
(28) Mühlbacher, D.; Scharber, M.; Morana, M.; Zhu, Z. G.; Waller, D.; Gaudiana, R.; Brabec, C. *Adv. Mater.* **2006**, *18*, 2884–2889.
(29) Bürgi, L.; Sirringhaus, H.; Friend, R. H. *Appl. Phys. Lett.* **2002**, *80*, 2913–2915.
(30) Sirringhaus, H. *Adv. Mater.* **2005**, *17*, 2411–2425.
(31) Coropceanu, V.; Cornil, J.; da Silva Filho, D. A.; Olivier, Y.; Silbey, R.; Brédas, J.-L. *Chem. Rev.* **2007**, *107*, 926–952.
(32) Osaka, I.; Zhang, R.; Sauv, G.; Smilgies, D.-M.; Kowalewski, T.; McCullough, R. D. *J. Am. Chem. Soc.* **2009**, *131*, 2521–2529.
(33) Zhang, W.; Li, J.; Zou, L.; Zhang, B.; Qin, J.; Lu, Z.; Poon, Y. F.; Chan-Park, M. B.; Li, C. M. *Macromolecules* **2008**, *41*, 8953–8955.
(34) Chabinyc, M. L.; Toney, M. F.; Kline, R. J.; McCulloch, I.; Heeney, M. *J. Am. Chem. Soc.* **2007**, *129*, 3226–3237.
(35) Kline, R. J.; McGehee, M. D.; Toney, M. F. *Nat. Mater.* **2006**, *5*, 222–228.
(36) Salleo, A. *Mater. Today* **2007**, *10*, 38–45.
(37) Kline, R. J.; McGehee, M. D. *Polym. Rev.* **2006**, *46*, 27–45.
(38) McCulloch, I.; et al. *Adv. Mater.* **2009**, *21*, 1091–1109.
(39) Brown, S. P.; Spiess, H. W. *Chem. Rev.* **2001**, *101*, 4125–4155.
(40) Brown, S. P. *Prog. Nucl. Magn. Reson. Spectrosc.* **2007**, *50*, 199–251.
(41) Hansen, M. R.; Graf, R.; Sekharan, S.; Sebastiani, D. *J. Am. Chem. Soc.* **2009**, *131*, 5251–5256.
(42) Feike, M.; Demco, D. E.; Graf, R.; Gottwald, J.; Hafner, S.; Spiess, H. W. *J. Magn. Reson., Ser. A* **1996**, *122*, 214–221.
(43) Feike, M.; Graf, R.; Schnell, I.; Jager, C.; Spiess, H. W. *J. Am. Chem. Soc.* **1996**, *118*, 9631–9634.
(44) Lazzeretti, P. *Prog. Nucl. Magn. Reson. Spectrosc.* **2000**, *36*, 1–88.
(45) Schnell, I.; Spiess, H. W. *J. Magn. Reson.* **2001**, *151*, 153–227.
(46) Schnell, I. *Prog. Nucl. Magn. Reson. Spectrosc.* **2004**, *45*, 145–207.
(47) Beaujuge, P. M.; Pisula, W.; Tsao, H. N.; Ellinger, S.; Müllen, K.; Reynolds, J. R. *J. Am. Chem. Soc.* **2009**, *131*, 7514–7515.
(48) Ong, B. S.; Wu, Y.; Liu, P.; Gardner, S. *J. Am. Chem. Soc.* **2004**, *126*, 3378–3379.
(49) Kim, Y.; Cook, S.; Tuladhar, S. M.; Choulis, S. A.; Nelson, J.; Durrant, J. R.; Bradley, D. D. C.; Giles, M.; McCulloch, I.; Ha, C.-S.; Ree, M. *Nat. Mater.* **2006**, *5*, 197–203.
(50) Zhang, M.; Tsao, H. N.; Pisula, W.; Yang, C.; Mishra, A. K.; Müllen, K. *J. Am. Chem. Soc.* **2007**, *129*, 3472–3473.
(51) Wang, C.; Jimison, L. H.; Goris, L.; McCulloch, I.; Heeney, M.; Ziegler, A.; Salleo, A. *Adv. Mater.* **2010**, *22*, 697–701.
(52) Pingel, P.; Zen, A.; Abellón, R. D.; Grozema, F. C.; Siebbeles, L. D. A.; Neher, D. *Adv. Funct. Mater.* **2010**, *20*, 2286–2295.
(53) He, M.; Li, J.; Sorensen, M. L.; Zhang, F.; Hancock, R. R.; Fong, H. H.; Pozdin, V. A.; Smilgies, D.-M.; Malliaras, G. G. *J. Am. Chem. Soc.* **2009**, *131*, 11930–11938.
(54) Pan, H.; Li, Y.; Wu, Y.; Liu, P.; Ong, B. S.; Zhu, S.; Xu, G. *J. Am. Chem. Soc.* **2007**, *129*, 4112–4113.
(55) McCulloch, I.; Heeney, M.; Bailey, C.; Genevicius, K.; Macdonald, I.; Shkunov, M.; Sparrowe, D.; Tierney, S.; Wagner, R.; Zhang, W.; Chabinyc, M. L.; Kline, R. J.; McGehee, M. D.; Toney, M. F. *Nat. Mater.* **2006**, *5*, 328–333.
(56) Brinkmann, M.; Rannou, P. *Adv. Funct. Mater.* **2007**, *17*, 101–108.
(57) Zen, A.; Saphiannikova, M.; Neher, D.; Grenzer, J.; Grigorian, S.; Pietsch, U.; Asawapirom, U.; Janietz, S.; Scherf, U.; Lieberwirth, I.; Wegner, G. *Macromolecules* **2006**, *39*, 2162–2171.
(58) Liu, J.; Zhang, R.; Osaka, I.; Mishra, S.; Javier, A. E.; Smilgies, D. M.; Kowalewski, T.; McCulloch, R. D. *Adv. Funct. Mater.* **2009**, *19*, 3427–3434.
(59) Osaka, I; Zhang, R.; Sauvé, G.; Smilgies, D. M.; Kowalewski, T.; McCulloch, R. D. *J. Am. Chem. Soc.* **2009**, *131*, 2521–2529.
(60) Prins, P.; Grozema, F. C.; Schins, J. M.; Patil, S.; Scherf, U.; Siebbeles, L. D. A. *Phys. Rev. Lett.* **2006**, *96*, 146601.